

Two-particle entanglement in capacitively coupled Mach-Zehnder interferometers

A.A. Vyshnevyy^a, A.V. Lebedev^b, G.B. Lesovik^c, and G. Blatter^b

^a*Department of general and applied physics, MIPT,*

Institutskii per. 9, 141700 Dolgoprudny, Moscow region, Russia

^b*Theoretische Physik, Wolfgang-Pauli-Strasse 27, ETH Zurich, CH-8093 Zürich, Switzerland and*

^c*L.D. Landau Institute for Theoretical Physics, RAS, 119334 Moscow, Russia*

(Dated: May 27, 2021)

We propose and analyze a mesoscopic device producing on-demand entangled pairs of electrons. The system consists of two capacitively coupled Mach-Zehnder interferometers implemented in a quantum Hall structure. A pair of electron wave-packets is injected into the chiral edge states of two (of the four) incoming arms; scattering on the incoming interferometers splits the wave-packets into four components of which two interact. The resulting interaction phase associated with this component leads to the entanglement of the state; the latter is scattered at the outgoing beam splitter and analyzed in a Bell violation test measuring the presence of particles in the four outgoing leads. We study the two-particle case and determine the conditions to reach and observe full entanglement. We extend our two-particle analysis to include the underlying Fermi seas in the quantum Hall device; the change in shape of the wave-function, the generation of electron-hole pairs in the interaction regime, and a time delay between the pulses all reduce the degree of visible entanglement and the violation of the Bell inequality, effects which we analyze quantitatively. We determine the device settings optimizing the entanglement and the Bell test and find that violation is still possible in the presence of the Fermi seas, with a maximal Bell parameter reaching $\mathcal{B} = 2.18 > 2$ in our setup.

PACS numbers: 73.23.-b, 03.67.Bg, 85.35.Ds, 73.43.Lp

I. INTRODUCTION

Quantum entanglement is a genuine property of quantum mechanics that has attracted a lot of attention recently due to its potential usefulness as a computational resource. As was first noticed by Bell¹, entangled states can violate a certain type of inequality expressed in terms of the correlation functions of measured outcomes. Later, Clauser and coworkers² suggested a more transparent inequality which was experimentally violated by photonic entangled states³.

The controlled creation and manipulation of *electronic* entangled states in solid state devices is a challenging problem and no experimental demonstration of a Bell inequality violation with electrons is available so far. The main challenge lies in the fact that, in contrast to photons, electrons are charged particles and thus strongly interact with the electromagnetic environment, leading to a fast decay of the coherence of the entangled state. On the other hand, the Coulomb interaction allows one to easily create entanglement among electrons.

During the last decade, several strategies have been suggested to create entangled states of ballistically propagating electrons in mesoscopic devices. The initial proposal was to use the generic spin-singlet entanglement of Cooper pairs in a superconductor^{4,5}, where the constituent electrons of a Cooper pair are injected into two different normal leads where they can propagate and thereby separate ballistically. Recently, the adiabatic splitting of Cooper pairs into normal conductors has been demonstrated experimentally⁶. The constituents of Cooper-pairs are entangled both in the orbital (energies) and spin degrees of freedom. The advantage of the spin-entanglement over the orbital entanglement is that the

spin coherence time can approach about 1 ms in semiconductor devices. However, the reliable demonstration of spin entanglement between electrons in a Bell test⁷ requires the detection of spin polarized currents at arbitrary polarization angles, that is still beyond the level of present technology. Alternatively, one can use the energy degrees of freedom of the injected Cooper pairs as an entangled variable⁸. The corresponding Bell test then requires the measurement of time-resolved current correlators on the GHz scale in the frequency domain.

Other proposals for two-electron entanglement make use of interacting quantum dot systems in the Coulomb blockade regime⁹ or ballistic electrons in integer quantum Hall devices^{10,11}. The latter proposals involve the entanglement of the electrons' orbital degrees of freedom and the corresponding Bell test requires the measurement of spinless current correlators among different leads of the setup. However, in contrast to the setups in Refs. 4,5,9, in these schemes the entanglement is produced due to a postselection at the moment of measurement and no interaction among electrons is required, see Refs. 12 for the discussion of the role of projection. In the postselection schemes, entangled states are produced with less than 100 % efficiency, in contrast to the proposals using interactions, where the entangled states are prepared deterministically by the unitary evolution.

Another disadvantage in the above proposals is that they operate at finite bias voltage where Cooper pairs or electrons are injected stochastically into the device. As a result the Bell test requires the measurement of current correlators at short times (of the order of the voltage time $\propto \hbar/eV$). To go beyond the short time limit, one alternatively can operate in the tunneling regime where electrons are injected rarely and one can measure correla-

tors at larger times $\propto \hbar/(TeV)$ (T is the transparency of the injecting lead). However, actual applications rely on the controlled creation of entangled states on demand. It was suggested in Ref. 13 to use Lorentzian voltage pulses to inject electron pairs on demand; the Bell test then requires only the detection of the total number of the transmitted particles through the different leads of the setup, and no short-time analysis is needed. The controlled injection of individual electrons into a device has been achieved recently, see Ref. 14.

Considerable progress has been made in the fabrication of electronic Mach-Zehner interferometers where electronic transport occurs through the edge states of an integer quantum Hall state. Experiments^{15,16} have uncovered an Aharonov-Bohm interference pattern at high visibility $\sim 62\%$. Later, the interference of two independent electrons coming from different sources has been reported¹⁷, reproducing the original Hanbury Brown and Twiss experiment in optics with a visibility approaching 70%.

Several theoretical proposals have been made to use coupled electronic Mach-Zehner interferometers to entangle two^{18,19} or three independent electrons²⁰. All these proposals deal with an idealized situation where only two or three electrons are present in the setup. However in real experiments^{15,16}, a non-monotonic dependence of the visibility factor has been observed at high bias voltages, that cannot be explained within a framework of non-interacting electron transport. Thus, the electron interaction cannot be ignored and indeed its proper accounting²¹ is required in order to explain the experimental data.

The purpose of the present work is to analyse an entangling device for (two) electrons consisting of two coupled Mach-Zehner interferometers, where electrons are injected on demand on top of the filled Fermi sea. In contrast to earlier proposals¹⁸⁻²⁰, here the injected electrons are interacting not only with each other but also with the underlying Fermi sea, leading to a parasitic entanglement with the surrounding electronic environment. We formulate the corresponding Bell inequality test and find the dependence of the Bell parameter \mathcal{B} as a function of the Coulomb interaction strength, the energy of the injected electrons, and the ratio between the mutual and self-capacitances of the interacting leads. As expected, the interaction with the Fermi sea leads to a strong decoherence and renders the Bell inequality violation more challenging (but still doable) as compared with the idealized two-electron situation: injecting narrow (high-energy) wave packets and for a mutual capacitance surpassing the self-capacitance of the interacting leads we find that a Bell parameter $\mathcal{B} \approx 2.18 > 2$ violating the Bell inequality $\mathcal{B} < 2$ can be reached.

In the following, we first discuss our setup and define our goals, the calculation of the maximally possible Bell parameter quantifying the entanglement in the wave function and the implementation of the Bell test with the expected outcomes for \mathcal{B} . In Section III we discuss the

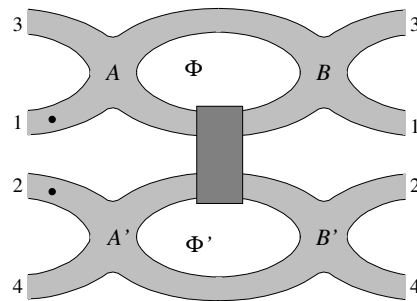


FIG. 1: Two Mach-Zehner interferometers capacitively coupled via the arms 1 and 2. Lorentzian-shaped pulses are injected into the left arms, entangled through the Coulomb interaction, and analyzed in a Bell test on the outgoing channels. In spite of the decoherence generated by the presence of the Fermi sea, the Bell inequality can be violated, demonstrating the possibility to generate ‘useful’ entanglement correlations in this setup.

Bell test with only two particles in the setup. The analysis is extended to include the underlying Fermi seas in the device in Section IV and we conclude in Sec. V. Technically, our analysis makes use of the fact that the effects of capacitive interaction between chiral electrons can be described by the action of voltage pulses²².

II. BELL SETUP

We consider two Mach-Zehner interferometers, the upper with leads ‘1’ and ‘3’ and a lower one with leads ‘2’ and ‘4’, where the two adjacent arms ‘1’ and ‘2’ are capacitively coupled, see Fig. 1. Each interferometer consists of two non-reflecting incoming and outgoing beam splitters A (A') and B (B') for the upper (lower) interferometer. The beam splitters A and B (A' and B') can be described by the unitary transfer matrices $\hat{t}(\alpha)$, $\hat{t}(\beta)$ ($\hat{t}(\alpha')$, $\hat{t}(\beta')$) in the lead basis $\{‘1’, ‘3’\}$ ($\{‘2’, ‘4’\}$), with

$$\hat{t}(\alpha) = \begin{bmatrix} \cos \alpha & -\sin \alpha \\ \sin \alpha & \cos \alpha \end{bmatrix} \quad (1)$$

parameterized by the angle α and corresponding expressions for the other matrices.

We describe the interaction between the electrons propagating in the adjacent leads ‘1’ and ‘2’ by the Hamiltonian

$$\hat{H}_{\text{int}} = \frac{1}{2} \sum_{i,j \in \{1,2\}} E_{ij} \hat{N}_i \hat{N}_j, \quad (2)$$

where $\hat{N}_i = \int dx \kappa_i(x) : \hat{\Psi}_i^\dagger(x) \hat{\Psi}_i(x) :$ is the excess electron number in a finite region of lead i defined by the coordinate kernel $\kappa_i(x)$ localized near the origin. We also use the notation $: \hat{A} := \hat{A} - \langle vac | \hat{A} | vac \rangle$ with $|vac\rangle$ denoting the ground state of the system. The coupling matrix \hat{E} describes the coupling constants due to the self-capacitances of the interferometer arms (diagonal terms

E_{11} and E_{22}) and due to the mutual capacitance between the adjacent arms of the different interferometers (off-diagonal terms $E_{12} = E_{21}$). For simplicity, we assume no interaction in the other leads ‘3’ and ‘4’, $E_{33} = E_{44} = 0$.

The excess electron charges are injected into the interferometers in a well defined non-entangled quantum state. Due to the particle interaction, the outgoing state becomes orbitally entangled (in the particle number measured in the outgoing leads) and this entanglement can be detected by performing a Bell test and observing the degree of violation of the corresponding CHSH-inequality. In the following, we formulate the Bell inequality in terms of cross-correlators $\langle \hat{N}_i \hat{N}_j \rangle$ ($i \in \{‘1’, ‘3’\}$ and $j \in \{‘2’, ‘4’\}$) between the number of excess particles transmitted through the different outgoing leads of the setup, $\hat{N}_i = \int dt : \hat{\Psi}_i^\dagger(x, t) \hat{\Psi}_i(x, t) :$. These correlators can be tuned by changing the magnetic fluxes Φ and Φ' penetrating each interferometer as well as the angles β and β' of the outgoing beam splitters (we will use symmetric splitters with $\alpha = \alpha' = \pi/4$ in the incoming leads). Defining the Bell correlator

$$E_{\beta\beta'}(\Phi, \Phi') = \frac{\langle (\hat{N}_1 - \hat{N}_3)(\hat{N}_2 - \hat{N}_4) \rangle}{\langle (\hat{N}_1 + \hat{N}_3)(\hat{N}_2 + \hat{N}_4) \rangle} \quad (3)$$

and the corresponding Bell observable,

$$\mathcal{B} = E_{\beta\beta'}(\Phi, \Phi') + E_{\beta\bar{\beta}'}(\Phi, \bar{\Phi}') + E_{\bar{\beta}\beta'}(\bar{\Phi}, \Phi') - E_{\bar{\beta}\bar{\beta}'}(\bar{\Phi}, \bar{\Phi}'), \quad (4)$$

one can formulate the two-party CHSH-inequality,

$$|\mathcal{B}| \leq 2. \quad (5)$$

The violation of the above inequality for some specific values of the magnetic fluxes $\vec{\Phi} = \{\Phi, \Phi', \bar{\Phi}, \bar{\Phi}'\}$ and angles $\vec{\beta} = \{\beta, \beta', \bar{\beta}, \bar{\beta}'\}$ quantifies the entanglement shared between the two interferometers. We will show that violation (although not maximal in the full setup including the Fermi surfaces) can be attained by changing only the magnetic fluxes at fixed (optimal) values of the beam splitter angles, $\beta = \bar{\beta}$ and $\beta' = \bar{\beta}'$, reducing the number of adjustable parameters, that might be helpful in a realistic experiment.

The actual value of the Bell parameter depends on the settings of the Bell test, the magnetic fluxes $\vec{\Phi}$ and the adjustment of the outgoing beam splitters defined by the angles $\vec{\beta}$: $\mathcal{B} = \mathcal{B}(\vec{\Phi}, \vec{\beta})$. In order to find the optimal setting of the Bell test where the Bell parameter attains its maxima, one needs to maximize $\mathcal{B}(\vec{\Phi}, \vec{\beta})$ as a function of all tuning parameters in the test. It has been shown in Ref. 23 that this optimization problem can be done analytically by calculating the two-particle density matrix of the entangled particles. We define the two-particle density matrix for our setup by placing the outgoing beam splitters B and B' into the asymptotic region where $\kappa_{1,2}(x) \rightarrow 0$ with no interaction present (as described by the limit $x \rightarrow +\infty$). In this region (before

the second beam splitters B and B'), the (many-particle) entangled scattering state $|BB'\rangle$ freely propagates in the positive direction and we define the (reduced) density matrix

$$[\hat{\rho}_{BB'}]_{ii'jj'} \propto \int dx dy \langle BB' | \hat{\Psi}_i^\dagger(x) \hat{\Psi}_{i'}^\dagger(y) \times \hat{\Psi}_{j'}(y) \hat{\Psi}_j(x) | BB' \rangle, \quad (6)$$

where $\hat{\Psi}_i(x)$ denote the free single-particle electronic field operators in the internal arms of the interferometers with $i, j \in \{‘1’, ‘3’\}$ and $i', j' \in \{‘2’, ‘4’\}$. According to Ref. 23 the maximal value of the Bell parameter is given by,

$$\mathcal{B}_{\max}(\hat{\rho}_{BB'}) = 2\sqrt{\lambda_1 + \lambda_2}, \quad (7)$$

where λ_1 and λ_2 are the two largest eigenvalues of the 3×3 symmetric matrix $\hat{T}_{\rho_{BB'}}^\dagger \hat{T}_{\rho_{BB'}}$ with $[\hat{T}_\rho]_{nm} = \text{Tr} \{ \hat{\rho} \cdot (\hat{\sigma}_n \otimes \hat{\sigma}_m) \}$ and where $\hat{\sigma}_n$, $n, m \in \{x, y, z\}$ are the Pauli matrices.

The phase accumulation due to magnetic fluxes Φ, Φ' and the scattering on the outgoing beam splitters act as a unitary rotation of the 4×4 density matrix,

$$\hat{\rho}_{BB'} \rightarrow \hat{\rho}_{\text{out}} = \hat{U}(\Phi, \beta, \Phi', \beta') \hat{\rho}_{BB'} \hat{U}^\dagger(\Phi, \beta, \Phi', \beta') \quad (8)$$

in the lead (or pseudo-spin) basis. This unitary rotation does not change the entanglement of the state since it involves only independent single-particle rotations in each interferometer, $\hat{U}(\Phi, \beta, \Phi', \beta') = \hat{U}(\Phi, \beta) \otimes \hat{U}(\Phi', \beta')$ where,

$$\hat{U}(\Phi, \beta) = \hat{t}(\beta) \begin{pmatrix} e^{i\Phi/2} & 0 \\ 0 & e^{-i\Phi/2} \end{pmatrix}. \quad (9)$$

Below, we will use Eq. (7) in order to find the maximal possible value of the Bell parameter in the device and Eq. (8) in order to calculate the Bell parameter (4) from the correlators (3).

III. BELL TEST WITH TWO ELECTRONS

We consider first the idealized situation where only two single-electron wave-packets are injected into the incoming leads ‘1’ and ‘2’ and no other electrons present in the system. The operator $\hat{f}_\alpha^\dagger = \int dx f(x) \hat{\Psi}_\alpha^\dagger(x)$ creates a single-particle state with wave-function $f(x)$ in lead α . Then, the incoming state with two wave-packets $f(x)$ and $g(x)$ in the leads ‘1’ and ‘2’ has the form, $|\text{in}\rangle = \hat{f}_1^\dagger \hat{g}_2^\dagger |\text{vac}\rangle$. After scattering on the incoming beam splitters A and A' , the wave-packets are split between the different internal arms of the interferometer. Before the wave-packets reach the interaction region the state of the system is a non-entangled product state,

$$|AA'\rangle = (\sin \alpha \hat{f}_3^\dagger + \cos \alpha \hat{f}_1^\dagger) \times (\sin \alpha' \hat{g}_4^\dagger + \cos \alpha' \hat{g}_2^\dagger) |\text{vac}\rangle. \quad (10)$$

Depending on the path chosen by the electrons, the various components of this product state evolve differently and the overall two-particle state becomes non-separable with respect to the different interferometers. For the empty vacuum state the interaction effects appear only in the scattering component where the electrons propagate through the adjacent arms '1' and '2'. Before the second beam splitters B and B' , the two-particle state has the form,

$$|BB'\rangle = [\cos \alpha \cos \alpha' (\hat{S} \hat{f}_1^\dagger \hat{g}_2^\dagger) + \sin \alpha \sin \alpha' (\hat{f}_3^\dagger \hat{g}_4^\dagger) + \sin \alpha \cos \alpha' (\hat{f}_3^\dagger \hat{g}_2^\dagger) + \cos \alpha \sin \alpha' (\hat{f}_1^\dagger \hat{g}_4^\dagger)] |vac\rangle, \quad (11)$$

where \hat{S} is the evolution operator corresponding to the interaction Hamiltonian (2). In order to find the scattering wave-function $\hat{S} \hat{f}_1^\dagger \hat{g}_2^\dagger |vac\rangle$ of the two electrons propagating in the interacting leads '1' and '2', we determine the eigenvalues and eigenvectors (ϵ_1, \vec{e}_1) and (ϵ_2, \vec{e}_2) of the coupling matrix \hat{E} in the interaction Hamiltonian (2) (note that the self-interaction terms have to be set to zero in the two-particle problem discussed here, $E_{ii} = 0$ for $i = 1, 2$). Introducing the electron number operators $\hat{n}_i = \sum_{j=1,2} e_{ij} \hat{N}_j$ (e_{ij} is the j -th component of the vector \vec{e}_i) one can rewrite the interaction Hamiltonian in the quadratic form,

$$\hat{H}_{\text{int}} = \frac{\epsilon_1}{2} \hat{n}_1^2 + \frac{\epsilon_2}{2} \hat{n}_2^2. \quad (12)$$

Next, we perform a Hubbard-Stratonovich transformation to decouple the charge operators \hat{n}_i (although not really necessary here, this procedure is convenient when dealing with the many electron case later on, see Appendix). The evolution operator then can be written in the form,

$$\hat{S} = \int Dz_1 Dz_2 \exp\left[\frac{i}{2} \int dt (\epsilon_1 z_1^2(t) + \epsilon_2 z_2^2(t))\right] \times \hat{T} \exp\left[-i \int dt (\epsilon_1 z_1(t) \hat{n}_1(t) + \epsilon_2 z_2(t) \hat{n}_2(t))\right], \quad (13)$$

where $z_{1,2}(t)$ are two real auxiliary fields obeying Gaussian statistics with $\langle z_i(t) z_j(t') \rangle = (i/\epsilon_i) \delta_{ij} \delta(t - t')$. This transformed evolution operator describes the independent propagation of two electrons in different leads, each subjected to a time-dependent scattering potential $V_i(x, t) = V_i(t) \kappa_i(x)$, $i = 1, 2$, with

$$V_i(t) = \epsilon_1 z_1(t) e_{1i} + \epsilon_2 z_2(t) e_{2i}. \quad (14)$$

Having mapped the two-particle evolution to two independent single-particle problems, we then solve the corresponding Schrödinger equations for the chiral electron modes with linear spectrum $\epsilon = v\hbar k$. The resulting two-particle wave-function $\Psi_{12}(x, y; t) = \langle x, y | \hat{S} \hat{f}_1^\dagger \hat{g}_2^\dagger |vac\rangle$ emerging behind the interaction region takes the form

$$\Psi_{12}(x, y; t) = f(x_t) g(y_t) \left\langle \exp\left\{-i \int^t dt' \times [V_1(t') \kappa_1(x_t + vt') + V_2(t') \kappa_2(y_t + vt')]\right\}\right\rangle, \quad (15)$$

where $x_t = x - vt$ and $y_t = y - vt$ are ballistically retarded variables, and the average has to be taken with respect to the Gaussian fields $z_i(t)$. Carrying out the averaging of the exponentials, we find the result

$$\Psi_{12}(x, y; t) = f(x_t) g(y_t) e^{-i\Phi_{12}(x, y)}, \quad (16)$$

$$\Phi_{12}(x, y) = E_{12} \int_0^\infty d\tau \kappa_1(x_\tau) \kappa_2(y_\tau). \quad (17)$$

The phase $\Phi_{12}(x, y)$ describes both the energy exchange and the deformation of the wave-functions $f(x)$ and $g(y)$ due to the interaction between the adjacent arms. In the end, the asymptotic ($t \rightarrow \infty$) form of the interacting component in the scattered state (11) is given by the expression

$$\hat{S} \hat{f}_1^\dagger \hat{g}_2^\dagger = \int dx dy f(x) g(y) e^{-i\Phi_{12}(x, y)} \hat{\Psi}_1^\dagger(x) \hat{\Psi}_2^\dagger(y). \quad (18)$$

Next, we calculate the two-particle density matrix (6) for the scattering state (11) inside the interferometer, $\hat{\rho}_{BB'} = \text{Tr}_{x, y} \{|BB'\rangle \langle BB'|\}$,

$$\hat{\rho}_{BB'} = (\hat{s}_\alpha \otimes \hat{s}_{\alpha'}) \begin{bmatrix} 1 & 1 & 1 & \mathcal{V} \\ 1 & 1 & 1 & \mathcal{V} \\ 1 & 1 & 1 & \mathcal{V} \\ \mathcal{V}^* & \mathcal{V}^* & \mathcal{V}^* & 1 \end{bmatrix} (\hat{s}_\alpha \otimes \hat{s}_{\alpha'}), \quad (19)$$

with $\hat{s}_\alpha = \text{diag}\{\sin \alpha, \cos \alpha\}$ and

$$\mathcal{V} = \int dx dy |f(x)|^2 |g(y)|^2 e^{-i\Phi_{12}(x, y)}. \quad (20)$$

We choose a particular form of the interaction kernels, $\kappa_1(x) = \kappa_2(x) = \exp(-|x|/a)$, where $2a$ is the length of the interaction region. Then the asymptotic form of the phase $\Phi_{12}(x, y)$ at $x, y \rightarrow +\infty$ is given by,

$$\Phi_{12}(x, y) = \varphi_0 \exp\left(-\frac{|x-y|}{a}\right) \left(1 + \frac{|x-y|}{a}\right), \quad (21)$$

with

$$\varphi_0 = \frac{E_{12} \tau_0}{\hbar} \quad (22)$$

the interaction-induced phase accumulated by the particles during the simultaneous propagation through the interaction region; here, $\tau_0 = a/v$ denotes the ballistic travelling time through the interaction region. We consider the case of simultaneous injection and choose incoming wave-packets of Lorentzian form with $\xi > 0$,

$$f(x) = g(x) = \sqrt{\frac{\xi}{\pi}} \frac{1}{x + i\xi}. \quad (23)$$

Then the parameter \mathcal{V} can be expressed as a function of two dimensionless parameters, the phase φ_0 , see Eq. (22), measuring the strength of the Coulomb interaction,

and $\gamma = \xi/a$ quantifying the width of the incoming wave-packet,

$$\mathcal{V}(\varphi_0, \gamma) = \int \frac{dx}{\pi} \frac{\exp[-i\varphi_0 e^{-2\gamma|x|}(1 + 2\gamma|x|)]}{x^2 + 1}. \quad (24)$$

Consider first the situation with infinitely narrow incoming wave-packets ($\gamma \rightarrow 0$) simultaneously injected into the device. The relevant values of the phase $\Phi_{12}(x, y)$ in \mathcal{V} are those near $x \approx y$, $\Phi_{12}(x, x) = \varphi_0$, resulting in

$$\mathcal{V}(\varphi_0, 0) \rightarrow \exp(-i\varphi_0), \quad (25)$$

see Eqs. (20) and (21) (when the wave-packets are injected with a time delay τ_d , the phase $\varphi_c \sim \Phi_{12}(v\tau_d) \sim \varphi_0 \exp(-v\tau_d/a)$ is reduced). The density matrix (19) corresponds to a pure state with $\hat{\rho}_{BB'}^2 = \hat{\rho}_{BB'}$. According to Eq. (7), the maximal value of the Bell parameter is given by,

$$\mathcal{B}_{\max} = 2\sqrt{1 + \sin^2(2\alpha) \sin^2(2\alpha') \sin^2 \frac{\varphi_0}{2}}. \quad (26)$$

The maximal violation $\mathcal{B}_{\max} = 2\sqrt{2}$ is attained for symmetric incoming beam splitters with $\alpha = \alpha' = \pi/4$ and $\varphi_0 = \pi$, requiring proper tuning of the interaction domain.

Next, we determine the optimal configurations of magnetic fluxes and angles $(\Phi, \bar{\Phi}, \beta, \bar{\beta})$ and $(\Phi', \bar{\Phi}', \beta', \bar{\beta}')$ for the upper and lower interferometer where the Bell inequality is maximally violated (we consider only the setup with symmetric incoming beam splitters). To do so, we derive the explicit form of the Bell correlation function $E_{\beta\beta'}(\Phi, \Phi')$, see Eq. (3). The correlation functions $\langle \hat{N}_i \hat{N}_{i'} \rangle$ entering into E are given by the diagonal elements of the two-particle density matrix $\hat{\rho}_{\text{out}}$ after scattering at the outgoing beam splitters, see Eq. (8). Then the Bell correlation function (3) assumes the form (we can set $\beta = \bar{\beta}$ and $\beta' = \bar{\beta}'$ and still violate the Bell inequality maximally)

$$\begin{aligned} E &= \frac{1}{2} \sin 2\beta \cos 2\beta' [V \cos(\Phi + \varphi_c) - \cos \Phi] \\ &+ \frac{1}{2} \cos 2\beta \sin 2\beta' [V \cos(\Phi' + \varphi_c) - \cos \Phi'] \\ &- \frac{1}{2} \sin 2\beta \sin 2\beta' [V \cos(\Phi + \Phi' + \varphi_c) + \cos(\Phi - \Phi')], \end{aligned} \quad (27)$$

where $V = |\mathcal{V}|$ and $\varphi_c = -\arg \mathcal{V}$. For infinitely narrow wave-packets simultaneously injected into the device, we have $V = 1$ and $\varphi_c = \varphi_0$, see Eq. (25). The Bell parameter then takes the form

$$\begin{aligned} \mathcal{B} &= 2[\sin 2\beta \cos 2\beta' \sin \Phi + \cos 2\beta \sin 2\beta' \sin \Phi'] \sin \frac{\varphi_c}{2} \\ &+ \sin 2\beta \sin 2\beta' [\cos \Phi \cos \Phi' + \cos \bar{\Phi} \cos \bar{\Phi}' \\ &\quad + \cos \Phi \cos \bar{\Phi}' - \cos \bar{\Phi} \cos \Phi'], \end{aligned} \quad (28)$$

where we have shifted all fluxes by $\varphi_c/2$, $\Phi \rightarrow \Phi + \varphi_c/2$ and so on. The maximal violation Eq. (26) is reached when

$$(\Phi, \bar{\Phi}) \rightarrow (\pi/2, 0), \quad (\Phi', \bar{\Phi}') \rightarrow (0, \pi) \quad (29)$$

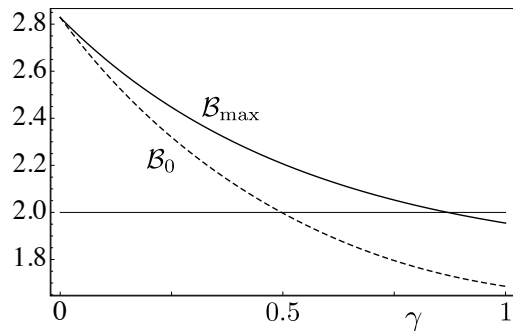


FIG. 2: Bell parameters \mathcal{B}_{\max} and \mathcal{B}_0 as a function of of width parameter $\gamma = \xi/a$ at $\varphi_0 = \pi$ for an optimal setting of Bell parameters (\mathcal{B}_{\max} , solid line) as given by Eq. (7) and for the non-optimal settings in Eq. (29) (\mathcal{B}_0 , dashed line).

and with angles $\beta = \pi/4$ and $\beta' = \text{arctg}[\sin(\varphi_c/2)]/2$ for the outgoing beam splitters. Note, that one can approach the maximal violation fixing the angles β and β' of the beam splitters to the above values and changing only the magnetic fluxes.

In a next step, we consider the situation where the incoming wave-packets have a finite width and thus a finite γ . Here, in contrast to the $\xi \rightarrow 0$ case, the interaction deforms the initial shape of the single particle wave-functions. This deformation appears only when both electrons are transmitted through the interacting arms '1' and '2' and is absent in the other scattering channels. Thus the orbital entanglement in the scattering (or pseudo-spin) degrees of freedom is recorded in the specific form of the orbital wave-functions. Since our detection scheme captures only the total number of the transmitted particles and is insensitive to the specific shape of the wave-packets, the reduced density matrix $\hat{\rho}_{BB'}$ in Eq. (19) is mixed and the pseudo-spin entanglement is reduced (for the case of narrow wave-packets with $\xi \rightarrow 0$, the tracing over x and y generates a mixed state as well, but does not reduce the entanglement which is only in the lead-indices). A further reduction in entanglement of extended wave packets is due to the electrons not meeting each other in the finite-range interaction region, thereby reducing their effective interaction.

When discussing the quantitative result for the Bell test with finite-width wave packets, we first analyze the value of the Bell parameter for the settings (29) which have been optimized for the $\gamma = 0$ case,

$$\mathcal{B}_0 = (1 + V) \sqrt{1 + \sin^2 \frac{\varphi_c}{2}}. \quad (30)$$

In the most favorable situation where $\varphi_c = \pi$, the Bell inequality cannot be violated for $V < \sqrt{2} - 1$. In reality, the interaction phase φ_c monotonically decreases from π as γ increases; in the limiting case of spatially extended wave-packets $\gamma \rightarrow \infty$, the electrons are unlikely to meet each other in the interaction region and $\varphi_c \rightarrow 0$.

The settings in Eq. (29), however, are not optimal

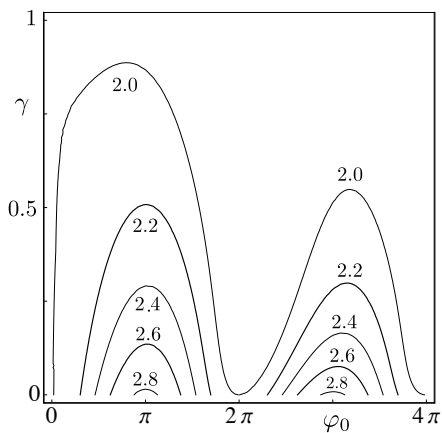


FIG. 3: Contour plot of the Bell parameter \mathcal{B}_{\max} for optimal settings of the Bell parameters as a function of the interaction parameter φ_0 (horizontal axis) and the width parameter γ (vertical axis). For small-width, high-energy wave packets ($\gamma \rightarrow 0$) the Bell inequality is maximally violated for odd multiples of π .

when γ is finite. In Fig. 2, we compare the maximal possible value of the Bell parameter \mathcal{B}_{\max} deriving from Eq. (7) with the non-optimal value \mathcal{B}_0 as given by Eq. (30) choosing an interaction parameter $\varphi_0 = \pi$. We find that $\mathcal{B}_{\max} > \mathcal{B}_0$ and the Bell inequality can be violated as long as $\gamma < \gamma_c \approx 0.87$ (the critical value for \mathcal{B}_0 is $\gamma_c \approx 0.497$).

The maximal value of the Bell parameter in the entire parameter space (φ_0, γ) is shown in Fig. 3. The region where the Bell inequality is violated ($\mathcal{B} > 2$) is shrinking as the strength of the Coulomb interaction (as encoded in φ_0) grows. Indeed, for a finite γ , a stronger interaction implies a larger deformation of the wave-packets and thus more pseudo-spin entanglement is recorded in the shape of the wave-packets. As a result, the detectable pseudo-spin entanglement is reduced, thus lowering the Bell inequality violation. On the contrary, for $\gamma = 0$, the maximal Bell parameter is a periodic function of φ_0 with maxima at $\varphi_0 = \pi, 3\pi, \dots$, see Eq. (26).

IV. BELL EXPERIMENT WITH FERMI SEA

We now extend our analysis to the more realistic situation including the (zero temperature) Fermi sea. First, we study the scattering problem where a single-particle Lorentzian wave-packet crosses an interaction region in a *single* lead. This problem has been studied before in Ref. 22 and we restate the results here. Next, we consider the scattering of two Lorentzian wave-packets propagating in two adjacent interacting leads and make use of these results to find a many-electron scattering state in the complete system with two coupled Mach-Zehnder interferometers. Knowledge of this state then permits us to determine the level of Bell inequality violation reachable

in the presence of a Fermi sea.

A. Scattering of a single wave-packet

Consider a single-electron state with a wave-function $f(x)$ created at $t_0 \rightarrow -\infty$ in the interaction-free asymptotic region of a one-dimensional conductor,

$$|f\rangle = \int dx f(x) \hat{\Psi}^\dagger(x, t_0) |\Phi_F\rangle, \quad (31)$$

where $|\Phi_F\rangle$ is the zero-temperature Fermi sea. We assume that all Fourier components of $f(x) = \sum_k f_k e^{ikx}$ are vanishing below the Fermi momentum, $f_k = 0$ for $k < k_F$. For the specific case of a Lorentzian wave packet, see Eq. (23), the incoming state $|f\rangle$ can be created by applying a local voltage pulse of Lorentzian shape,

$$V(t) = \frac{2\hbar}{e\tau} \frac{1}{1 + (t - t_0)^2/\tau^2}, \quad (32)$$

in the asymptotic region $x_0 \rightarrow -\infty$ of the conductor; here $\tau = \xi/v_F$ is the duration of the pulse²⁴. Then the state $|f\rangle$ can be written as²⁵,

$$|f\rangle = \hat{U}[\phi(t)] \hat{F}^\dagger |\Phi_F\rangle, \quad (33)$$

where \hat{F}^\dagger is an electron ladder operator increasing the number of electrons in the system by one. The unitary operator $\hat{U}[\phi]$ describes the evolution of the wave function under the action of the Lorentzian voltage pulse (32) applied at the position $x = x_0$,

$$\hat{U}[\phi] = \hat{T}_+ \exp \left[i v_F \int dt \phi(t) \hat{\rho}(x_0, t) \right], \quad (34)$$

with \hat{T}_+ the forward time-ordering operator, $\hat{\rho}(x, t) = : \hat{\Psi}^\dagger(x, t) \hat{\Psi}(x, t) :$ the electron density operator, and $\phi(t) = \int^t dt' eV(t')/\hbar$ is the phase accumulated by the electrons.

The wave packet then propagates ballistically towards the interaction region around $x = 0$ and arrives there at $t = 0$, assuming $x_0 = v_F t_0$. Due to the interaction, the excess electron can exchange energy with the Fermi sea, thereby exciting electron-hole pairs. Subsequently, this many-particle scattering state (the excess electron plus the electron-hole cloud) ballistically propagates to the interaction-free region at large $x \rightarrow +\infty$ where it assumes the form

$$|\tilde{f}\rangle = \hat{T}_+ \exp \left[-\frac{i}{\hbar} \int_{-\infty}^{\infty} dt \hat{H}_{\text{int}}(t) \right] |f\rangle, \quad (35)$$

with \hat{H}_{int} given in Eq. (2).

At first glance the scattering state $|\tilde{f}\rangle$ should be a rather complicated entangled state involving an excess electron and additional electron-hole pairs. However, the central result of Ref. 22 says that the state $|\tilde{f}\rangle$ can again

be produced by applying an additional voltage pulse $V_\chi(t)$ to the incoming state $|f\rangle$, $|\tilde{f}\rangle = \hat{U}[\chi]|f\rangle$, with $\chi(t) = \int^t dt' e V_\chi(t')/\hbar$. The remarkable consequence of this fact is that the scattering state has the form of a simple Slater determinant and is in fact non-entangled, since it can be produced by an evolution operator generated by a single particle Hamiltonian.

The peculiarity of the Lorentzian incoming state becomes clear when one goes to the bosonic formulation, expressing the fermionic field operator through bosonic creation/annihilation operators \hat{b}_k^\dagger and \hat{b}_k , $\hat{\Psi}(x) \propto \exp[i \sum_{k>0} (\hat{b}_k e^{ikx} + \hat{b}_k^\dagger e^{-ikx})/\sqrt{k}] \hat{F}$, see Appendix for details. Integrating over the coordinate in the definition of the incoming state (see Eq. (31)) with the Lorentzian form of $f(x)$, the wave-packet can be written in the form

$$|f\rangle \propto \exp\left(-i \sum_{k>0} \frac{e^{-k\xi}}{\sqrt{k}} \hat{b}_k^\dagger\right) \hat{F}^\dagger |\Phi_B\rangle, \quad (36)$$

where $|\Phi_B\rangle$ is the bosonic vacuum state. This state can be recognized as a coherent state of bosons $|f\rangle = \prod_{k>0} |v_k\rangle$ with amplitudes $v_k = -ie^{-k\xi}/\sqrt{k}$. In the bosonized picture any electron interaction of the form $V(x, y)\hat{\rho}(x)\hat{\rho}(y)$ is quadratic in bosonic variables and thus corresponds to a potential scattering of the bosons. Due to the chiral nature of the present scattering problem, the back reflection of bosons is forbidden and the only result of that scattering is the appearance of a momentum dependent forward scattering phase $\delta_{sc}(k)$, $\hat{b}_k \rightarrow \hat{b}_k \exp[i\delta_{sc}(k)]$, where the actual form of $\delta_{sc}(k)$ depends on the particular form of the interaction kernel $V(x, y)$. Hence, the scattered state of bosons is again a *coherent* state,

$$|\tilde{f}\rangle \propto \exp\left[-i \sum_{k>0} \frac{e^{-k\xi - i\delta_{sc}(k)}}{\sqrt{k}} \hat{b}_k^\dagger\right] \hat{F}^\dagger |\Phi_B\rangle. \quad (37)$$

Going back to the electronic picture, this scattered state can again be created by applying a corresponding voltage pulse $\tilde{V}(t)$ given by

$$\tilde{V}(t) = \frac{\hbar}{e} \int_0^\infty d\omega \exp[-\tau\omega + i\delta_{sc}(\omega/v_F) + i\omega t] + C.c. \quad (38)$$

Even more, for an initial voltage pulse of arbitrary form, the generated state $|f_U\rangle = \hat{U}[\phi]\hat{F}^\dagger|\Phi_F\rangle$ can be represented as a coherent bosonic state as well, $|f_U\rangle = \prod_{k>0} e^{u_k \hat{b}_k - u_k^* \hat{b}_k^\dagger} \hat{F}^\dagger |\Phi_B\rangle$ with amplitudes $u_k = v_F \sqrt{k} \phi(kv_F)/2\pi$ determined by the Fourier transform $\phi(\omega)$ of the phase $\phi(t) = \int^t dt' e V(t')/\hbar$. The voltage pulse $\tilde{V}(t)$ generating the wave function behind the scatterer then derives from the phase $\tilde{\phi}(\omega) = \phi(\omega) \exp[i\delta_{sc}(\omega/v_F)]$.

B. Scattering of two wave-packets

Let us next analyse the scattering problem for two electron wave-packets propagating in the two adjacent interacting leads ('1' and '2') of the upper and lower interferometer (unprimed and primed). We assume that initially at $t_0 \rightarrow -\infty$ the incoming state is given by,

$$|fg\rangle = \int dx dx' f(x)g(x') \hat{\Psi}_1^\dagger(x, t_0) \hat{\Psi}_2^\dagger(x', t_0) |\Phi_F\rangle. \quad (39)$$

In order to generalize the result of the previous section to the case of the two-particle scattering problem, we calculate the overlap of the scattered state $|\tilde{f}\tilde{g}\rangle = \hat{S}|fg\rangle$ and the state $|fg\rangle_U$ (for later convenience we use χ and χ' referring to the upper and lower interferometers rather than the lead indices '1' and '2'),

$$|fg\rangle_U = \hat{U}_1[\chi] \hat{U}_2[\chi'] |fg\rangle, \quad (40)$$

obtained by applying two distinct voltage pulses $V_\chi(t)$ and $V_{\chi'}(t)$ in the corresponding (upper and lower) leads to the incoming state $|fg\rangle$ in the *non-interacting* system. The overlap,

$$\mathcal{O}_{fg}[\chi(t), \chi'(t)] = \langle fg | \hat{U}_1^\dagger[\chi] \hat{U}_2^\dagger[\chi'] \hat{S} | fg \rangle, \quad (41)$$

is a function of the phases $\chi(t)$ and $\chi'(t)$ and we want to find its maxima, $\mathcal{O}_{fg} = \max_{\chi, \chi'} |\mathcal{O}[\chi, \chi']|$ as a function of phases $\chi(t)$ and $\chi'(t)$.

As shown in the Appendix, there exist particular phases $\chi(t)$ and $\chi'(t)$ producing an overlap (41) of unit magnitude, provided that the incoming wave-packets $f(x)$ and $g(x)$ have a Lorentzian form (the more general statement actually is that one can reach full overlap for *any* voltage-pulse generated incoming states). Thus we conclude that the scattered state $|\tilde{f}\tilde{g}\rangle = \hat{S}|fg\rangle$ can be obtained by applying two voltage pulses to the incoming state of the non-interacting problem,

$$\hat{S}|fg\rangle = \exp(i\Phi) \hat{U}_1[\chi(t)] \hat{U}_2[\chi'(t)] |fg\rangle \quad (42)$$

with Φ an overall phase. As a result, the scattered state is a Slater determinant and thus is non-entangled.

In the following, we assume for simplicity that the interacting leads are characterized by the same coordinate kernels $\kappa_1(x) = \kappa_2(x) = \kappa(x)$. Let $\vec{e}_\nu = \{e_{\nu 1}, e_{\nu 2}\}$ and ϵ_ν , $\nu = 1, 2$, be the eigenvectors and corresponding eigenvalues of the coupling matrix of the interaction Hamiltonian Eq. (2). Provided the wave-packets $f(x)$ and $g(x)$ are Lorentzians with widths ξ_1 and ξ_2 , the interaction equivalent phases $\chi(t)$ and $\chi'(t)$ have Fourier components of the form,

$$\chi(\omega > 0) = e_{11}(e_{11}e^{-\omega\tau_1} + e_{12}e^{-\omega\tau_2})F_1(\omega) + e_{21}(e_{21}e^{-\omega\tau_1} + e_{22}e^{-\omega\tau_2})F_2(\omega), \quad (43)$$

$$\chi'(\omega > 0) = e_{12}(e_{11}e^{-\omega\tau_1} + e_{12}e^{-\omega\tau_2})F_1(\omega) + e_{22}(e_{21}e^{-\omega\tau_1} + e_{22}e^{-\omega\tau_2})F_2(\omega), \quad (44)$$

with $\chi(-\omega) = \chi^*(\omega)$ and the same for $\chi'(\omega)$ and the overall phase reads

$$\Phi = - \sum_{i=1,2} \int_0^\infty \frac{d\omega}{2\pi} \left[v_F^2 \text{Re}[G_{++}(\omega)] |F_i(\omega)|^2 + \text{Re}[F_i(\omega)] \right] (e_{i1}e^{-\omega\tau_1} + e_{i2}e^{-\omega\tau_2})^2, \quad (45)$$

where $\tau_{1,2} = \xi_{1,2}/v_F$. The functions $F_i(\omega)$ are given by

$$F_i(\omega) = \frac{\epsilon_i |\kappa(\omega)|^2}{1 - i\epsilon_i \Pi_{++}^*(\omega)}, \quad (46)$$

with $\kappa(\omega) = \int dt \kappa(v_F t) e^{-i\omega t}$, $\Pi_{++}(\omega) = \int dx dx' \kappa(x) \kappa(x') G_{++}(\omega, x, x')$ and $G_{++}(\omega, x, x')$ is the Fourier transform of the Green's function $G_{++}(\tau, x, x') = \langle \hat{T}_+ \{ \hat{\rho}(x, \tau) \hat{\rho}(x', 0) \} \rangle$,

$$G_{++}(\omega, x, x') = \frac{1}{2\pi v_F^2} \int \frac{d\omega'}{2\pi i} \frac{\omega' e^{-i\omega'(x-x')/v_F}}{\omega' - \omega - i\delta \text{sgn}(\omega)}. \quad (47)$$

C. The complete scattering state

Due to the self-capacitance of the interferometer arms, electron-hole pairs can be excited in scattering processes where only one wave-packet (the upper or lower) propagates through the corresponding interacting arm of the interferometer. The corresponding interaction equivalent fields χ and χ' and the overall phase Φ can be formally found from Eqs. (43)–(45) by setting the width of the absent wave-packet to infinity, $\xi_1 \rightarrow \infty$ or $\xi_2 \rightarrow \infty$. In the following, we introduce a new notation for the interaction equivalent fields in the upper (χ_{ij}) and lower (χ'_{ij}) interferometer and for the overall phase (Φ_{ij}), where the indices $i, j \in \{0, 1\}$ tell whether a particle has moved through the upper ($i = 1$) or lower ($j = 1$) lead (else $i, j = 0$ if there is no particle in the lead). The scattering state inside the interferometers before the outgoing beam splitters B and B' then takes the form (we assume symmetric incoming beam splitters with $\alpha = \alpha' = \pi/4$; note that the operators \hat{U} always act on the interacting leads ‘1’ and ‘2’),

$$\begin{aligned} |BB'\rangle = & \frac{1}{2} [\hat{f}_3^\dagger \hat{g}_4^\dagger + e^{i\Phi_{11}} \hat{U}_1[\chi_{11}] \hat{U}_2[\chi'_{11}] \hat{f}_1^\dagger \hat{g}_2^\dagger \\ & + e^{i\Phi_{10}} \hat{U}_1[\chi_{10}] \hat{U}_2[\chi'_{10}] \hat{f}_1^\dagger \hat{g}_4^\dagger \\ & + e^{i\Phi_{01}} \hat{U}_1[\chi_{01}] \hat{U}_2[\chi'_{01}] \hat{f}_3^\dagger \hat{g}_2^\dagger] |\Phi_F\rangle. \end{aligned} \quad (48)$$

Each of the four scattered- or pseudo-spin components corresponds to a Slater determinant state and thus does not exhibit any interaction-induced entanglement. However, the overall state cannot be factorized with respect to the upper and lower interferometer degrees of freedom

because each component is formally obtained under a different evolution (different interaction-equivalent phases). Hence, the interaction induces pseudo-spin entanglement between the non-entangled many-particle electron-hole cloud states.

Before evaluating the Bell inequalities for the full setup including the Fermi sea, we first wish to gauge our expectations with a discussion of the degree of entanglement we can expect in our two Mach-Zehnder interferometers. Our Bell test is sensitive only to the excess particle number transmitted through a given outgoing lead. In order to describe the statistics of the Bell test, it is sufficient to know the reduced 4×4 density matrix $\hat{\rho}_{BB'}$ obtained from the *full* density operator $\hat{\rho}_{\text{ud}} = |BB'\rangle\langle BB'|$ by tracing out all spatial degrees of freedom, see Eq. (6). Formally, this corresponds to dividing all degrees of freedom into the (observable) pseudo-spin degrees of freedom associated with finding a particle in the leads ‘1’ or ‘3’ (encoded by B) or in the leads ‘2’ or ‘4’ (encoded in B') plus all the remaining degrees of freedom (we encode these with the letter R), hence $\hat{\rho}_{BB'} = \text{Tr}_R |BB'\rangle\langle BB'|$. In a first step, we then can calculate the von Neumann entropy $S(\hat{\rho}_{BB'}) \equiv -\text{Tr}[\hat{\rho}_{BB'} \log_2(\hat{\rho}_{BB'})]$ of the measured outcomes. This entropy ranges between 0 and 2 and tells us about the degree of entanglement between the pseudo-spin degrees of freedom and the rest of the system. A value $S(\hat{\rho}_{BB'}) = 0$ tells us, that R is not entangled with the pseudo-spin system BB' and hence the system BB' can be maximally entangled; on the contrary, a value $S(\hat{\rho}_{BB'}) = 2$ informs us that R is fully entangled with BB' and all information about the latter is encoded in R . Due to the monogamy of entanglement, the two subsystems B and B' cannot be entangled in this case. Indeed, calculating the reduced density matrices $\hat{\rho}_B = \text{Tr}_{B'}[\rho_{BB'}]$ and $\hat{\rho}_{B'} = \text{Tr}_B[\rho_{BB'}]$ and the associated entropy $S(\hat{\rho}_B) \equiv -\text{Tr}[\hat{\rho}_B \log_2(\hat{\rho}_B)]$ (and similar for B') we expect that $S(\hat{\rho}_B)$ ranges between 0 (B not entangled with B') and 1 (B maximally entangled with B') if $S(\hat{\rho}_{BB'}) = 0$, while $S(\hat{\rho}_B) = 0$ if $S(\hat{\rho}_{BB'}) = 2$.

Hence, the more degrees of freedom from R that are entangled with B or B' we integrate out (as we do not observe them in our Bell test), the smaller is the remaining entanglement between B and B' and the weaker is the violation of the Bell test, see Fig. 4. Consider first the two-particle Bell test described in Sec. III. For narrow wave packets, the trace over the coordinates does

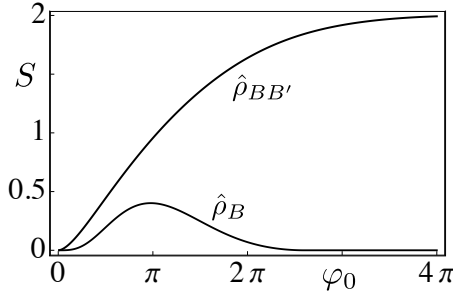


FIG. 4: Von Neumann entropy $S(\hat{\rho}_{BB'})$ of measured outcomes of the double Mach-Zehnder interferometer quantifying the entanglement with the unobserved degrees of freedom in the system. The entanglement increases with the interaction strength and the system is fully entangled with the environment at large φ_0 . The entropy $S(\hat{\rho}_B)$ expresses the entanglement *between* the two Mach-Zehnder interferometers and thus the potential for violation of the Bell test. Increasing the interaction first entangles the two MZ interferometers with each other but as the entire system gets entangled with the environment upon further increase of φ_0 , the entanglement between the interferometers decreases.

not reduce the entanglement in the outgoing leads (hence $S(\hat{\rho}_{BB'}) = 0$) and we expect the entropy $S(\hat{\rho}_B)$ to reach unity under ideal conditions where B and B' are fully entangled; we then can expect that the Bell inequality can be maximally violated. For extended wave packets, the spacial degrees of freedom are relevant, e.g., some ‘which-path’ information is stored in the shape of the wave-function in the outgoing channels. The entropy $S(\hat{\rho}_{BB'})$ does not vanish as the system BB' is entangled with R and hence the entropy $S(\hat{\rho}_B)$ cannot reach unity any more; the Bell inequality cannot be maximally violated any longer. Finally, including the Fermi sea, the entanglement between R and BB' is even larger since even further information on the BB' system is encoded in unobserved degrees of freedom in R , e.g., the presence of an additional hole in the outgoing channel tells, that the particles sure did not choose the paths ‘3’ and ‘4’, since no interaction is active in this case. As a consequence, $S(\hat{\rho}_{BB'})$ deviates more strongly from zero, $S(\hat{\rho}_B)$ is further reduced from unity, and the maximum in the Bell inequality violation is further diminished.

For a quantitative analysis, we then calculate the two-particle density matrix $\hat{\rho}_{BB'}$ corresponding to the state (48), see Eq. (6). The diagonal elements are all equal to $1/4$, while the remaining six independent elements are given by

$$[\hat{\rho}_{BB'}]_{12,14} = \frac{-1}{4\pi} \int \frac{\tau_2 dt}{\tau_2^2 + t^2} e^{i[\chi'_{11}]+(t)+i[\chi'_{10}]- (t)}, \quad (49)$$

$$[\hat{\rho}_{BB'}]_{12,32} = \frac{-1}{4\pi} \int \frac{\tau_1 dt}{\tau_1^2 + t^2} e^{i[\chi_{11}]+(t)+i[\chi_{01}]- (t)}, \quad (50)$$

$$[\hat{\rho}_{BB'}]_{12,34} = \frac{1}{4} \exp(i[\chi_{11}]+(i\tau_1) + i[\chi'_{11}]+(i\tau_2)), \quad (51)$$

$$[\hat{\rho}_{BB'}]_{14,34} = -\frac{1}{4} \exp(i[\chi_{10}]+(i\tau_1)), \quad (52)$$

$$[\hat{\rho}_{BB'}]_{32,34} = -\frac{1}{4} \exp(i[\chi'_{01}]+(i\tau_2)), \quad (53)$$

$$[\hat{\rho}_{BB'}]_{14,32} = \frac{1}{4} \left[\frac{1}{\pi} \int \frac{\tau_1 dt}{\tau_1^2 + t^2} e^{i[\chi_{10}]+(t)+i[\chi_{01}]- (t)} \right] \times \left[\frac{1}{\pi} \int \frac{\tau_2 dt}{\tau_2^2 + t^2} e^{-i[\chi'_{01}]- (t)-i[\chi'_{10}]+(t)} \right], \quad (54)$$

where $[f]_{\pm}(t)$ are the components of the function $f(t)$ analytical in the upper (lower) half plane,

$$[f]_{\pm}(t) = \pm \frac{1}{2\pi i} \int dt' \frac{f(t')}{t' - t \mp i0}. \quad (55)$$

For the sake of simplicity we assume a symmetric situation where the interacting leads have the same self-interaction $E_{11} = E_{22}$ and the wave-packets have the same form $f(x) = g(x)$ and thus $\tau_1 = \tau_2 = \tau$, implying that $[\hat{\rho}_{BB'}]_{12,14} = [\hat{\rho}_{BB'}]_{12,32}$ and $[\hat{\rho}_{BB'}]_{14,34} = [\hat{\rho}_{BB'}]_{32,34}$. We first focus on the situation of infinitely narrow wave-packets $\gamma = \xi/a \rightarrow 0$, allowing us to replace $\tau/(\tau^2 + t^2) \rightarrow \pi\delta(t)$ in Eqs. (49)–(54). The Bell correlation function then takes the form

$$E = \frac{V_1}{2} \sin 2\beta \cos 2\beta' [\cos(\Phi + \varphi_s + \varphi_c) - \cos(\Phi + \varphi_s)] + \frac{V_1}{2} \cos 2\beta \sin 2\beta' [\cos(\Phi' + \varphi_s + \varphi_c) - \cos(\Phi' + \varphi_s)] - \frac{1}{2} \sin 2\beta \sin 2\beta' [(V_1 V_2)^2 \cos(\Phi + \Phi' + 2\varphi_s + \varphi_c) + (V_1/V_2)^2 \cos(\Phi - \Phi')]. \quad (56)$$

Here, the phase $\varphi_c = \text{Re}[\chi_{01}]_+(t=0)$ assumes the role of φ_c in the two-particle case, the phase difference between the two cases where a particle traverses the lead ‘1’ with (χ_{11}) and without (χ_{10}) presence of a particle in lead ‘2’. Since $\chi_{11} = \chi_{10} + \chi_{01}$, it is the difference χ_{01} that enters into φ_c . The phase $\varphi_s = \text{Re}[\chi_{10}]_+(t=0)$ is due to the self-interaction of the particle passing through lead ‘1’; this phase is absent in the two-particle scattering problem. Finally, the visibility factors are given by $V_1 = \exp[-\text{Im}[\chi_{10}]_+(t=0)]$ (describing the situation where only one particle traverses the interaction region) and $V_2 = \exp[-\text{Im}[\chi_{01}]_+(t=0)]$ (showing up when both particles traverse the interaction region; no correlations appear in the absence of any interaction). Note that both factors $V_1 V_2 < 1$ and $V_1/V_2 < 1$.

The phase shift φ_s can be eliminated from Eq. (56) by incorporation in the magnetic fluxes and setting $\varphi_s = 0$. Let us then choose the same values of (renormalized) magnetic fluxes as for the two-particle case, Eq. (29); substituting the settings in Eq. (29) into Eq. (56), we find the Bell parameter

$$\mathcal{B} = 2V_1 \sqrt{V_1^2 \frac{(V_2^2 + V_2^{-2})^2}{4} + \sin^2 \frac{\varphi_c}{2}}, \quad (57)$$

at $\beta = \pi/4$ and $\cot 2\beta' = 2 \sin(\varphi_c/2)/(V_1(V_2^2 + V_2^{-2}))$. As before, we consider the interaction kernel $\kappa(x) =$

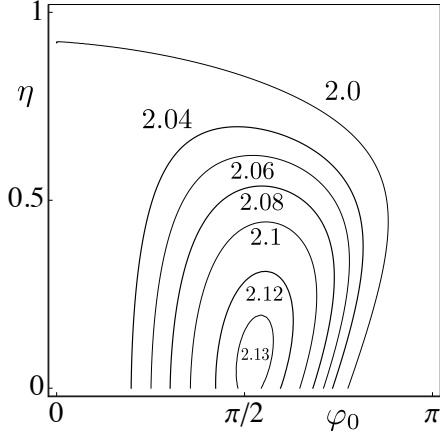


FIG. 5: Bell parameter (57) for the non-optimal settings of the Bell parameters in Eq. (29) as a function of interaction parameter φ_0 (horizontal axis) and the parameter η (vertical axis) describing the ratio of self- to mutual capacitance.

$\exp(-|x|/a)$ and relate the self-coupling constants E_{ii} to the mutual coupling parameter E_{12} via the dimensionless factor $\eta > 0$, $E_{11} = E_{22} = \eta E_{12}$. Then

$$\kappa(\omega) = \frac{2\tau_0}{1 + (\omega\tau_0)^2}, \quad (58)$$

and

$$\Pi_{++}(\omega) = -\frac{\tau_0}{2\pi i} \frac{1}{(\omega\tau_0 + i)^2}, \quad (59)$$

with $\tau_0 = a/v_F$ the ballistic traveling time through the interaction region. For the symmetric setup, the interaction equivalent phases obey the symmetry relations $\chi_{10} = \chi'_{01}$ and $\chi_{01} = \chi'_{10}$ with

$$\chi_{10}(t) = 4n_{10} \int d\nu \frac{e^{-|\nu|\gamma + i\nu t/\tau_0}}{(\nu + i)^2 [(\nu - i)^2 - n_{10}]}, \quad (60)$$

where $n_{10} = (\varphi_0/2\pi)(\eta+1)$, and similarly for the χ_{01} field with $n_{01} = (\varphi_0/2\pi)(\eta-1)$. In Fig. 5 we plot the value of the Bell parameter (57) as a function of φ_0 , see Eq. (22), and the parameter η . The maximal value $\mathcal{B} \approx 2.13$ violating the Bell inequality is assumed at $\varphi_0 \approx 0.53\pi$ and $\eta = 0.083$.

As noticed before, the settings (29) might be non-optimal in the general case. The full optimization of the Bell test according to Eq. (7) gives a higher value of the Bell parameter, see Fig. 6, where we find the maximal violation of the Bell inequality $\mathcal{B} \approx 2.18 > 2$ at $\varphi_0 \approx 0.73\pi$ and $\eta \approx 0.58$. Note that a value $\eta < 1$ implies that the self-capacitance is smaller than the mutual capacitance, $E_{22} < E_{12}$; we will discuss this point further below.

Above, we have concentrated on the case of infinitely narrow (or high energy) wave-packets, $\gamma = \xi/a \rightarrow 0$. The maximal value of the Bell parameter for the general situation with a finite-width wave-packet is shown in Fig.

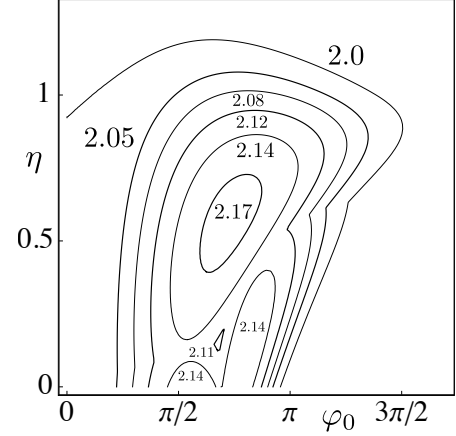


FIG. 6: Maximal value of the Bell parameter as a function of interaction parameter φ_0 (horizontal axis) and the parameter η describing the ratio of self- to mutual capacitance (vertical axis).

7, where we have chosen the optimal value $\eta = 0.58$ for narrow wave packets with $\gamma = 0$. We find that lowering the energy of the excess electrons decreases the value of the Bell parameter and using high-energy wave-packets happens to be the best operating limit for the Bell test.

The interaction-equivalent phase χ_{10} involves two dimensionless parameters, $\gamma = \xi/a$ and the Coulomb strength $\varphi_0 = E_{12}\tau_0/\hbar$. Using phase-space arguments, one can see that these parameters determine the number of excitations that can be created via the wave-packet's excess energy $\delta\epsilon_\xi = \hbar v_F/2\xi$ or via the Coulomb energy $\delta\epsilon_C = E_{12}$. Indeed, multiplying these energies by the density of states $\rho = 1/\hbar v_F$ and the length a , we obtain the number of electrons that can be excited within the interaction region, $N_\xi \sim a\rho\delta\epsilon_\xi = a/2\xi$ and $N_C = \delta\epsilon_C\tau_0/\hbar = \varphi_0$. The narrower the wave-packet is, the more electron-hole pairs can be excited. On the other hand, the finite Coulomb interaction strength restricts the number of excited particles to below N_C , no matter how narrow the incoming wave-packet is. As a result a further increase in the energy of the incoming particles beyond $\delta\epsilon_C$ is not harmful since it does not produce more electron-hole excitations and thus does not lead to a further reduction of the Bell parameter.

Decreasing the number of parasitic electron-hole pairs should be a good strategy to enhance the value of the Bell parameter. Keeping the interaction fixed (say, near $\varphi_0 = \pi$), one could choose spatially extended wave-packets such that N_ξ drops below N_C . In this situation the number of electron-hole pairs is defined by the smaller number N_ξ . However, for extended wave-packets with large ξ , the electrons are unlikely to meet each other in the interaction region, thereby decreasing the interaction phase, see Eq. (21). As a result of this trade-off, the Bell inequality can never be violated in this regime, though the number of parasitic electron-hole excitations is small. However, using extended wave-packets, one could count

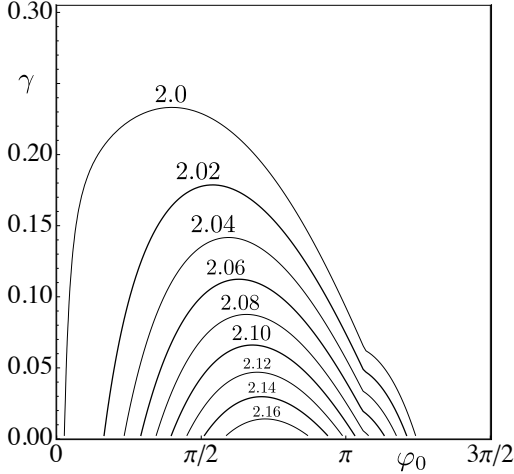


FIG. 7: Bell parameter (57) as a function of interaction parameter φ_0 (horizontal axis) and the width parameter $\gamma = \xi/a$ (vertical axis) at $\eta = 0.58$.

the particles in the outgoing leads within a finite time window δt , $\hat{N}_i(t) = \int_{t-\delta t/2}^{t+\delta t/2} dt \hat{I}_i(t)$, thus projecting the electron trajectories on the component where the electrons have passed the interaction region simultaneously. For $\xi > a$, the number of excited electron-hole pairs is limited by $N_\xi \ll 1$ and one can observe a sufficient violation of the Bell inequality. In this approach, however, the entanglement is likely to be induced by the projection (or the Bell measurement) itself and the setup cannot be used as a genuine source of entangled particles.

So far, our results have been obtained for the specific form of the interaction kernel $\kappa(x) = \exp(-|x|/a)$ with smooth tails. A different form of $\kappa(x)$ may result in a different value of the maximal Bell parameter. To check how strongly the result depends on the shape of $\kappa(x)$, we consider another kernel $\kappa(x) = 1$ for $x \in [-a, a]$ and 0 otherwise. This kernel has sharp edges and generates an interaction equivalent phase of the form

$$\chi_{10}(t) = 4n_{10} \int d\nu \frac{\sin^2 \nu}{\nu} \frac{e^{-|\nu|\gamma + i\nu t/\tau_0}}{\nu - in_{10}(1 - e^{-2i\nu})} \quad (61)$$

and similarly for the phase χ_{01} with $n_{10} \rightarrow n_{01}$, see Eq. (60). The numerical analysis for high-energy wave packets ($\gamma \rightarrow 0$) produces a maximal value of the Bell parameter $\mathcal{B} \approx 2.15$ which is assumed at lower interaction $\varphi_0 \approx 0.34\pi$ and a similar value $\eta \approx 0.53$.

Finally, we discuss the capacitive Hamiltonian (2) used throughout the discussion. In a realistic situation the injected electrons experience a Coulomb interaction which is screened by the Fermi sea when propagating through the adjacent interaction leads. The peculiarity of the edge states of the Quantum Hall system is that the edge state $\varphi_k(y) e^{ikx}$ with a wave-vector $k > 0$ has a transverse

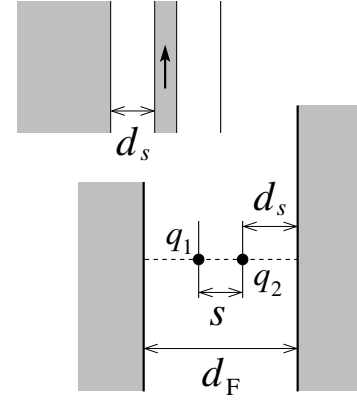


FIG. 8: Interaction region between edge states ‘1’ and ‘2’ in a quantum Hall device. The edge states are separated from the closest screening Fermi sea by a distance $d_s \approx \ell^2/\xi$ (top left). We model the capacitive interaction Hamiltonian (2) by analyzing two charges q_1 and q_2 separated by s and screened by metallic plates at a distance d_F .

component

$$\varphi_k(y) = H_n \left(\frac{y + k\ell^2}{\ell} \right) \exp \left(-\frac{(y + k\ell^2)^2}{\ell^2} \right) \quad (62)$$

which is spatially separated by $k\ell^2$ from the Fermi sea electrons occupying states with $k < 0$, see Fig. 8 (here $\ell = \sqrt{\varphi_0}/2\pi B$ is the cyclotron length and $H_n(y)$ are Hermite polynomials; we assume a flat boundary potential). Denoting by d_F the distance between the two Fermi seas, Lorentzian wave-packets with a small width ξ then can be brought close to each other, with a distance $d_F - 2d_s$ between the two wave packets and a distance $d_s \approx \ell^2/\xi$ from the nearest Fermi surface screening the interaction.

We model this situation by two parallel grounded metallic gates (accounting for the screening effect of the Fermi seas in the adjacent interacting arms) separated by a distance d_F with two charges q_1 and q_2 at a separation $s < d_F$ and located symmetrically along a line perpendicular to the metallic plates. The electrostatic energy of this system is given by,

$$E(q_1, q_2) = \frac{E_{11}}{2} q_1^2 + E_{12} q_1 q_2 + \frac{E_{22}}{2} q_2^2, \quad (63)$$

with coupling constants ($E_{11} = E_{22}$)

$$E_{ii} = \frac{1}{d_F} \left[\psi \left(\frac{1+\alpha}{2} \right) + \psi \left(\frac{1-\alpha}{2} \right) - 2\psi(1) \right], \quad (64)$$

$$E_{12} = \frac{1}{d_F} \left[2\psi \left(\frac{1}{2} \right) - \psi \left(1 + \frac{\alpha}{2} \right) - \psi \left(1 - \frac{\alpha}{2} \right) + \frac{1}{\alpha} \right],$$

where $\psi(x)$ is the digamma function and $\alpha = s/d_F$. The last term $\propto 1/\alpha$ in the off-diagonal coupling strength E_{12} is the direct Coulomb interaction $q_1 q_2/s$ of the two charges. It is this term which allows to realize a situation where $|E_{12}| > |E_{11}|$ when $\alpha < 0.177$.

V. CONCLUSION

We have studied the on-demand generation of entangled electron pairs in a double Mach-Zehnder interferometer implemented in a quantum Hall setting; the entanglement is generated via the capacitive interaction between two neighboring interferometer arms, shifting the phase of one wave-function component with respect to the other. The resulting entangled state is analyzed in a Bell test measuring the particle numbers in the outgoing leads; the second beam splitters and the fluxes threading the interferometers serve to define the four measuring conditions (polarizations) in the Bell test.

Our first study with only two electrons present in the device serves to identify the optimal conditions to generate full entanglement and maximal violation of the Bell test in the simplest situation. We find that simultaneous injection of high-energy pairs provides the best conditions for entanglement; broad (low-energy) wave-packets reduce the probability that the electrons meet and interact, as does a delay between the particles. Furthermore, extended wave-functions are deformed in the interaction region and thus transfer ‘which-path’ information to the outgoing leads. Since our Bell test is sensitive only to the particle number in the outgoing leads, this (discarded) wave-function deformation entails a reduction of violation in the Bell test.

Including the Fermi sea, decoherence and additional ‘which-path’ information due to the generation of electron-hole pairs within the interaction region are expected to further reduce the entanglement in the relevant degrees of freedom, the particle numbers measured in the outgoing leads. The most important question addressed in the present work then is: can such an idealized device generate sufficient entanglement to be observed in a Bell test? We find that this is indeed the case, provided the capacitive coupling between the two arms can be implemented such that the mutual interaction dominates over the self-interaction.

In our work we consider electrons in chiral states of a quantum Hall device and a purely capacitive (in particular, non-resistive) coupling. Technically, this allows for the bosonization of the scattering problem describing the interaction region (however, not the scattering at

the beam splitters), which is at the heart of transforming an incoming Slater determinant into an outgoing Slater determinant; this allows us to describe the effect of the interaction via a voltage-pulse, thus replacing an apparent many-body problem by a single-particle evolution. Physically, this implies that the decoherence is reduced in our system and limited to the creation of particle-hole pairs. It turns out, that these particle-hole pairs further reduce (as compared with the two-particles case) the entanglement and the violation in the Bell test, but to a limited degree, still providing a violation $\mathcal{B} \approx 2.18 > 2$ in an optimized situation. Regarding the experimental implementation, we refer the reader to the layout described in Ref. 16. A favorable finding is that the Bell test can be performed by only changing the fluxes through the loops (possibly by using a side gate deforming the loop area) and does not require tuning of the beam splitters. An interesting further element is, how correction pulses resurrecting the wave function behind the scatterer as described in Ref. 22 can help to restore a higher degree of Bell-inequality violation.

We acknowledge financial support from the Swiss National Science Foundation through the National Center of Competence in Research on Quantum Science and Technology (QSIT), the Pauli Center for Theoretical Studies at ETH Zurich, and the RFBR Grant No. 11-02-00744-a.

Appendix A: Wave packet scattering

We show that the scattering state of two Lorentzian wave-packets $f_{1,2}(x)$ propagating along two interacting adjacent leads ‘1’ and ‘2’ is indeed described by a Slater determinant state and thus can be prepared by applying an evolution operator generated by a single-particle Hamiltonian. We assume that this single-particle evolution can be generated by voltage pulses, i.e., the Hamiltonian accounts for the interaction of the electrons with voltage pulses applied at $x = 0$ and adds the time dependent phases $\chi(t)$ and $\chi'(t)$ to the state in the leads ‘1’ and ‘2’, see Eq. (34). In order to demonstrate that there are specific phases $\chi(t)$ and $\chi'(t)$ generating the scattering state, we need to calculate the overlap,

$$\mathcal{O} = \int dx_1 dx_2 f_1^*(x_1) f_2^*(x_2) \int dx'_1 dx'_2 f_1(x'_1) f_2(x'_2) \langle \hat{\Psi}_2(x_2, t_0) \hat{\Psi}_1(x_1, t_0) \hat{U}_1^\dagger[\chi] \hat{U}_2^\dagger[\chi'] \hat{S} \hat{\Psi}_1^\dagger(x'_1, t_0) \hat{\Psi}_2^\dagger(x'_2, t_0) \rangle, \quad (\text{A1})$$

and show, that there exist phases $\chi(t)$ and $\chi'(t)$ such that the modulus $|\mathcal{O}|$ reaches unity. In Eq. (A1), $t_0 \rightarrow -\infty$ and the averaging is taking over zero temperature Fermi sea. In order to calculate the overlap, we can make use of the Green’s function,

$$\mathcal{C}(12|1'2') = \langle T_K \{ \hat{U}_1[\chi(t^-)] \hat{U}_2[\chi'(t^-)] \hat{S}_+ \hat{\Psi}_2(x_2, t_0^-) \hat{\Psi}_1(x_1, t_0^-) \hat{\Psi}_1^\dagger(x'_1, t_0^+) \hat{\Psi}_2^\dagger(x'_2, t_0^+) \} \rangle, \quad (\text{A2})$$

where we have introduced the Keldysh time ordering T_K and have defined the fields $\chi(t)$ and $\chi'(t)$ on the lower

branch of the Keldysh contour (going back in time), while

the evolution operator

$$\hat{S}_+ = \hat{T}_K \exp \left[-\frac{i}{\hbar} \int_{-\infty}^{+\infty} dt \hat{H}_{\text{int}}(t^+) \right] \quad (\text{A3})$$

is defined on the upper branch of the Keldysh contour (forward in time).

We decouple the quadratic interaction Hamiltonian (2) with the Hubbard-Stratonovich transform Eq. (13) and obtain the evolution operator \hat{S}_+ in the form

$$\begin{aligned} \hat{S}_+ &= \int Dz_1(t) Dz_2(t) \hat{S}_1[\tilde{z}_1] \hat{S}_2[\tilde{z}_2] \\ &\times \exp \left[\frac{i}{2} \int dt [\epsilon_1 z_1^2(t) + \epsilon_2 z_2^2(t)] \right], \end{aligned} \quad (\text{A4})$$

where the real fields $z_{1,2}(t)$ are non-zero on the upper branch of the Keldysh contour. The actions (see Eq. (12) for the definition of n_i)

$$\hat{S}_i[\tilde{z}_i] = T_K \exp \left[-i \int dt \tilde{z}_i(t) \hat{n}_i(t) \right], \quad i = 1, 2, \quad (\text{A5})$$

with $\tilde{z}_i(t) = \epsilon_1 z_1(t) e_{1i} + \epsilon_2 z_2(t) e_{2i}$, describe the forward in time evolution of the electrons in the leads $i = 1, 2$ under the action of the time dependent fields $\tilde{z}_i(t)$ acting

within the interaction region according to the Hamiltonians $\hat{H}_{z_i}(t) = \int dx \tilde{z}_i(t) \kappa(x) \hat{\rho}_i(x)$. The Green's function (A2) can be factorized with respect to the leads,

$$\mathcal{C}(12|1'2') = \langle \mathcal{C}(1|1') \mathcal{C}(2|2') \rangle_{\tilde{z}_1, \tilde{z}_2}, \quad (\text{A6})$$

where the average is taken over the fields $\tilde{z}_{1,2}$ and

$$\begin{aligned} \mathcal{C}(xt_0|x't_0) &= \langle T_K \{ \hat{U}[\chi^-] \hat{S}[\tilde{z}^+] \\ &\times \hat{\Psi}(x, t_0^-) \hat{\Psi}^\dagger(x', t_0^+) \} \rangle \end{aligned} \quad (\text{A7})$$

with $\hat{S}[\tilde{z}^+]$ the action in the relevant lead. Next, we make use of the bosonization technique, see Ref. 25 for details, and express the density operator $\hat{\rho}(x, t)$ through the chiral bosonic field $\hat{\rho}(x, t) = \partial_x \hat{\theta}(x - v_F t) / 2\pi$ where $\hat{\theta}(x) = -\sum_{k>0} (\hat{b}_k e^{ikx} + \hat{b}_k^\dagger e^{-ikx}) / \sqrt{k}$ and $\hat{b}_k^\dagger, \hat{b}_k$ are bosonic creation and annihilation operators obeying the standard commutation relation $[\hat{b}_k, \hat{b}_{k'}^\dagger] = \delta_{kk'}$. The electronic field operator $\hat{\Psi}(x)$ can be expressed through the field $\hat{\theta}(x)$ via $\hat{\Psi}(x) = \hat{F} e^{-i\hat{\theta}(x)} / \sqrt{2\pi\delta}$ with $\delta \rightarrow 0^+$ an ultraviolet cutoff and \hat{F} is a Klein factor acting as an electron-number ladder operator.

Calculating the bosonic averages in (A7), one arrives at the result

$$\begin{aligned} \mathcal{C}(\tau|\tau') &= \frac{1}{2\pi i v_F} \frac{e^{i[\chi]^+(\tau') + i[\chi]^-(\tau)}}{\tau - \tau' - i\delta} \exp \left\{ \int_0^\infty \frac{d\omega}{2\pi} \left[i\tilde{z}(\omega) \kappa^*(\omega) e^{i\omega\tau'} + i\tilde{z}^*(\omega) \kappa(\omega) (e^{-i\omega\tau} + i\omega\chi(\omega)/2\pi) \right. \right. \\ &\left. \left. - |\tilde{z}(\omega)|^2 \Pi_{++}(\omega) - v_F^2 |\chi(\omega)|^2 G_{++}^*(\omega) \right] \right\}, \end{aligned} \quad (\text{A8})$$

where we have introduced retarded variables $\tau = t_0 - x/v_F$ and $\tau' = t_0 - x'/v_F$; the quantities $G_{++}(\omega)$ and $\Pi_{++}(\omega)$ are defined in Eq. (47). Substituting this expression into Eq. (A6) and taking the Gaussian integrals over the fields $z_1(t)$ and $z_2(t)$, one finally arrives at the following expression for the correlation function $\mathcal{C}(12|1'2')$,

$$\begin{aligned} \mathcal{C}(12|1'2') &= \frac{e^{i[\chi]^+(\tau'_1) + i[\chi]^-(\tau_1) + i[\chi]^\dagger(\tau'_2) + i[\chi]^\dagger(\tau_2)}}{(2\pi i v_F)^2 (\tau_1 - \tau'_1 - i\delta)(\tau_2 - \tau'_2 - i\delta)} \exp \left[-v_F^2 \int_0^\infty \frac{d\omega}{2\pi} (|\chi(\omega)|^2 + |\chi'(\omega)|^2) G_{++}^*(\omega) \right] \\ &\times \prod_{k=1,2} \exp \left[-i \int_0^\infty \frac{d\omega}{2\pi} F_k^*(\omega) (e_{k1} e^{i\omega\tau'_1} + e_{k2} e^{i\omega\tau'_2}) (e_{k1} (e^{-i\omega\tau_1} + i\omega\chi(\omega)/2\pi) + e_{k2} (e^{-i\omega\tau_2} + i\omega\chi'(\omega)/2\pi)) \right], \end{aligned} \quad (\text{A9})$$

with the functions $F_k(\omega)$, $k = 1, 2$, defined in Eq. (46). This correlator is an analytic function of the retarded variables τ_1 and τ_2 (τ'_1 and τ'_2) in the lower (upper) half plane. This feature allows us to evaluate the integrals

over the coordinates in Eq. (A1) involving Lorentzian wave-packets with the widths ξ_1 and ξ_2 . In the end, we arrive at the following expression for the overlap

$$\mathcal{O} = \exp \left[i[\chi]_+(i\tau_{\xi_1}) + i[\chi]_-(-i\tau_{\xi_1}) + i[\chi']_+(i\tau_{\xi_2}) + i[\chi']_-(-i\tau_{\xi_2}) - v_F^2 \int_0^\infty \frac{d\omega}{2\pi} (|\chi(\omega)|^2 + |\chi'(\omega)|^2) G_{++}^*(\omega) \right] \\ \times \prod_{k=1,2} \exp \left[-i \int_0^\infty \frac{d\omega}{2\pi} F_k^*(\omega) (e_{k1} e^{-\omega\tau_{\xi_1}} + e_{k2} e^{-\omega\tau_{\xi_2}}) \left(e_{k1} (e^{-\omega\tau_{\xi_1}} + i\omega\chi(\omega)/2\pi) + e_{k2} (e^{-\omega\tau_{\xi_2}} + i\omega\chi'(\omega)/2\pi) \right) \right].$$

Minimizing the real part of the overall exponential provides the optimal fields χ and χ' in Eqs. (43) and (44)

producing a maximal overlap $|\mathcal{O}| = 1$; the overall phase is given by Eq. (45).

-
- ¹ J.S. Bell, *Physics* **1**, 195 (1964).
² J.F. Clauser, M.A. Horne, A. Shimony, and R.A. Holt, *Phys. Rev. Lett.* **23**, 880 (1969).
³ A. Aspect, P. Grangier, and G. Roger, *Phys. Rev. Lett.* **47**, 460 (1981).
⁴ G. Lesovik, T. Martin, and G. Blatter, *Eur. Phys. J. B* **24**, 287 (2001).
⁵ P. Recher, E. Sukhorukov, and D. Loss, *Phys. Rev. B* **63**, 165314 (2001).
⁶ L. Hofstetter, S. Csonka, J. Nygard, and C. Schönenberger, *Nature* **461**, 960 (2009); J. Wei and V. Chandrasekhar, *Nature Phys.* **6**, 494 (2010); A. Das, Y. Ronen, M. Heiblum, D. Mahalu, A.V. Kretinin, and H. Shtrikman, [arXiv:1205.2455](https://arxiv.org/abs/1205.2455).
⁷ N. Chtchelkatchev, G. Blatter, G. Lesovik, and T. Martin, *Phys. Rev. B* **66**, 161320 (2002).
⁸ K.V. Bayandin, G.B. Lesovik, and T. Martin, *Phys. Rev. B* **74**, 085326 (2006).
⁹ D.S. Saraga and D. Loss, *Phys. Rev. Lett.* **90**, 166803 (2003).
¹⁰ C.W.J. Beenakker *et al.*, *Phys. Rev. Lett.* **91**, 147901 (2003).
¹¹ P. Samuelsson, E.V. Sukhorukov, and M. Büttiker, *Phys. Rev. Lett.* **91**, 157002 (2003); *ibid* **92**, 026805 (2004).
¹² A.V. Lebedev, G. Blatter, C.W.J. Beenakker, and G.B. Lesovik, *Phys. Rev. B* **69**, 235312 (2004); A.V. Lebedev, G.B. Lesovik, and G. Blatter, *Phys. Rev. B* **71**, 045306 (2005).
¹³ A.V. Lebedev, G.B. Lesovik, and G. Blatter, *Phys. Rev. B* **72**, 245314 (2005).
¹⁴ G. Feve, A. Mahe, J.-M. Berroir, T. Kontos, B. Plaçaais, D.C. Glattli, A. Cavanna, B. Etienne, and Y. Jin, *Science* **316**, 1169 (2007).
¹⁵ Y. Ji, Y. Chung, D. Spinzak, M. Heiblum, D. Mahalu, and H. Shtrikman, *Nature (London)* **422**, 415 (2003).
¹⁶ P. Roulleau, F. Portier, D.C. Glattli, P. Roche, A. Cavanna, G. Faini, U. Gennser, and D. Mailly, *Phys. Rev. B* **76**, 161309 (2007); L.V. Litvin, H.-P. Tranitz, W. Wegscheider, and C. Strunk, *Phys. Rev. B* **75**, 033315 (2007).
¹⁷ I. Neder, N. Ofek, Y. Chung, M. Heiblum, D. Mahalu, and V. Umansky, *Nature (London)* **448**, 333 (2007).
¹⁸ Kicheon Kang and Kahnh Ho Lee, *Physica E* **40**, 1395 (2008).
¹⁹ J. Dressel, Y. Choi, and A.N. Jordan, *Phys. Rev. B* **85**, 045320 (2012).
²⁰ A.A. Vyshnevyy, G.B. Lesovik, T. Jonckheere, and T. Martin, [arXiv:1204.5850](https://arxiv.org/abs/1204.5850).
²¹ E.V. Sukhorukov and V.V. Cheianov, *Phys. Rev. Lett.* **99**, 156801 (2007); I.P. Levkivskyi and E.V. Sukhorukov, *Phys. Rev. B* **78**, 045322 (2008); I. Neder and E. Ginossar, *Phys. Rev. Lett.* **100**, 196806 (1008); D.L. Kovrizhin and J.T. Chalker, *Phys. Rev. B* **81**, 155318 (2010).
²² A.V. Lebedev and G. Blatter, *Phys. Rev. Lett.* **107**, 076803 (2011).
²³ R. Horodecki, P. Horodecki, and M. Horodecki, *Phys. Lett. A* **200**, 340 (1995).
²⁴ In the Hall-bar geometry, the chiral electrons move (along x) in the transverse potential ($U(y)$) generated by the gates and the Fermi velocity v_F should be replaced by the (local) drift velocity $v_{\text{drift}} \sim -\ell^2 [\partial_y U]_{y_0} / \hbar$, with y_0 the position of the edge channel.
²⁵ J. von Delft and H. Schoeller, *Ann. Phys. (Leipzig)* **7**, 225 (1998).